Journal of Materials Chemistry B

ROYAL SOCIETY OF CHEMISTRY

PAPER

View Article Online
View Journal

Cite this: DOI: 10.1039/d0tb00767f

Controlled release of small molecules and proteins from DNA-surfactant stabilized metal organic frameworks†

Mark Q. Tolentino, Alyssa K. Hartmann, David T. Loe and Jesssica L. Rouge *

Received 21st March 2020,
Accepted 1st May 2020

DOI: 10.1039/d0tb00767f

rsc.li/materials-b

This work highlights a multifunctional nanoscale material which can effectively compartmentalize small molecules and biomolecules into a single, micellar structure with programmable degradation properties resulting in highly controllable release properties. The nanomaterial consists of a ZIF-8 metal organic framework (MOF) encapsulated within a DNA surfactant micelle assembly, referred to as a nucleic acid nanocapsule (NAN). NANs have been demonstrated to enter cells through endocytosis and result in intracellular cargo release upon enzyme-triggered degradation. By combining the favorable properties of MOFs (large storage capacity) with those of NANs (triggerable release), we show diverse molecular cargo can be integrated into a single, highly programmable nanomaterial with controllable release profiles. The hybrid MOF–NANs exhibit double-gated regulation capabilities as evidenced by kinetic studies of encapsulated enzymes that indicate individual layers of the particle influence the overall enzymatic rate of turnover. The degradation of MOF–NANs can be controlled under multiple combined stimuli (*i.e.* varying pH, enzymes), enabling selective release profiles in solutions representative of more complex biological systems. Lastly, the enhanced control over the release of small molecules, proteins and plasmids, is evaluated through a combination of cell culture and *in vitro* fluorescence assays, indicating the potential of MOF–NANs for both therapeutic and diagnostic applications.

1. Introduction

Many nanoscale drug carriers are formulated from hydrophobic materials as most drug molecules for medical treatment are hydrophobic in nature.[1] To date, solubilizing traditionally insoluble drug molecules has been a major benefit of nanomaterial formulations such as micelle and lipid nanoparticles, owing to their hydrophobic and lipophilic interior compositions.[2,3] Despite these seemingly well matched systems, one aspect that remains challenging in drug delivery is the ability to encapsulate hydrophilic and larger therapeutically relevant biomacromolecules such as plasmids and proteins.[4–6] Recently, our group reported a nanocapsule system which can readily enter cells for the delivery of short, charged oligonucleotides and small hydrophobic molecules in a single structure we refer to as a nucleic acid nanocapsule (NAN).[7,8] The NAN design is inspired by spherical nucleic acid like structures that have been reported to have enhanced cellular uptake due to the presence of DNA at the surface of the particle that improves its uptake into cells by enabling endocytosis of the particle without the use of transfection agents.[9] An important feature that enables the NANs success is its controllable degradation in response to specific proteolytic enzymes within its cellular environment.[10]

Despite its programmable degradation properties, the current NAN formulation is limited in that it can only accommodate hydrophobic small molecules in its interior and short oligonucleotides on its exterior mostly due to chemical compatibility and stability limitations. Due to the growing interest in achieving controlled delivery of hydrophilic small molecules and larger biomacromolecules such as plasmids, mRNA, and proteins, we decided to investigate ways in which we could broaden the chemical nature of the cargo that the NAN could accommodate. To address these challenges, we began investigating metal organic frameworks (MOFs) as a modification to our NANs interior compartment (Fig. 1A). MOFs are well known for their ability to encapsulate a wide range of molecular cargo.[11–13] The Zeolite Imidazole Framework-8 (ZIF-8) MOF particularly stood out as a promising choice for our studies due to its small size and recent successes in biological applications.[14,15] The ZIF-8 framework is built from 2-methyl imidazole ligands and Zn^{2+} ions. It has been used to encapsulate a variety of small molecules, including dyes and drugs, as well as larger proteins and macromolecules.[16–21] More recently, protocols have been developed for making

Department of Chemistry, University of Connecticut, Storrs, CT 06269, USA. E-mail: jessica.rouge@uconn.edu

† Electronic supplementary information (ESI) available. See DOI: 10.1039/d0tb00767f

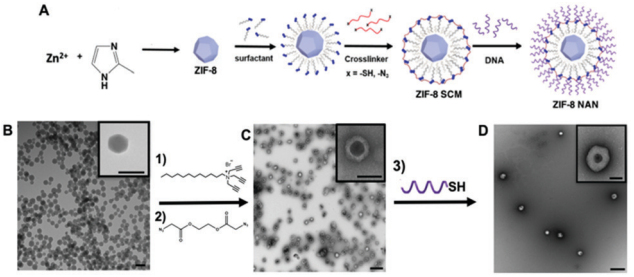

Fig. 1 Assembly and crosslinking of surfactant (1) around a ZIF-8 MOF. (A) Scheme showing the stepwise crosslinking of the micelle surface around the ZIF-8 MOF using either diazido crosslinkers or thiol-terminated crosslinkers. Thiolated DNA (3) is added to the alkyne modified surface through further surface functionalization using UV light and a photoinitiator. (B) TEM image of nanosized ZIF-8, scale bars are 100 nm. (C) TEM image of the same batch of ZIF-8 MOFs post encapsulation in surface crosslinked micelle (SCM), scale bars are 100 nm (inset) and 500 nm (zoomed out). (D) TEM image of ZIF-8 inside a nucleic acid nanocapsule (NAN) post DNA functionalization, scale bars are 100 nm (inset) and 500 nm (zoomed out). The dark outer lining originates from the staining of DNA on the surface of nanoparticle. All samples are stained with uranyl acetate to highlight the presence of the soft organic shell around the ZIF-8 MOF.

nanosized ZIF-8 MOFs that are sub-100 nm in size, in contrast to more traditional micron sized MOFs. Additionally, its components have been successfully used to mineralize proteins to enhance their stability in biological systems. For all of these reasons the ZIF-8 MOF is an excellent choice for encapsulation within our NANs, and well suited for downstream cellular uptake studies.

However, despite these attractive features, there are also certain limitations to using MOFs as biological delivery vehicles. Owing to their metal coordinated framework, ZIF-8 MOFs can be easily broken down using acidic conditions *via* protonation of the imidazole ligands. The acid labile nature of MOFs is a useful trigger for cargo release, as they have been shown to be taken into cells *via* endocytosis, resulting in their degradation in the acidic environment of endosomes.[22–24] Yet, despite this triggerable degradation, the overall instability of MOFs often leads to premature degradation,[25,26] likely due to multiple competing mechanisms that either protonate ligands or chelate the zinc ions. This presents a significant problem for MOFs as a material class for drug delivery and remains a significant hurdle facing their therapeutic and diagnostic potential.[27,28]

Premature degradation of MOFs can lead to leakage of toxic drug molecules prior to arriving at the intended cellular location, or the leakage of dyes preventing accurate tracking and signaling.[29,30]

To address concerns of MOF stability, cationic surfactants, such as cetyltrimethylammonium bromide (CTAB), have been incorporated at the exterior of MOFs.[31] In the context of biological systems, ZIF-8 MOFs were recently stabilized in cell media using polyvinyl pyrrolidone (PVP), which enabled prolonged stability of ZIF-8 encapsulated proteins within a MOF.[27] However, despite the added stability these approaches provide, the only trigger for cargo release remained the MOFs response to the acidic environment of the endosome, which lacks specificity for cell type. In the CTAB–MOF stability study (evaluated in non-biological systems), it is thought that the hydrophobic faces formed at the MOFs exterior imidazole rings serve as seeding sites for the assembly of the hydrophobic tails of CTAB molecules.[31] As our NAN formulation is also built from cationic surfactant precursors and is enzyme responsive, we decided to test whether we could utilize our crosslinked surfactant approach to not only improve the stability of the ZIF-8 MOFs for biological applications, but also to introduce a controllable degradation mechanism to the ZIF-8 MOFs beyond that of acidic protonation of imidazole ligands by using degradation and release in response to enzyme activity. An ideal trigger would be one that is more specific to the environment of the MOF within a given cell type or disease state.

In our current NAN design, the trigger for its degradation is the presence of specific cellular enzymes that are expressed either extracellularly or intracellularly. For example, we have synthesized peptide crosslinked NANs that degrade exclusively in the presence of matrix metalloprotease 9 (MMP9), an extracellular enzyme that is over expressed during periods of inflammation.[10] In our system the peptide crosslinkages block the release of small molecule drugs from leaking out of the NANs micelle core until they are degraded by a target enzyme. Similarly, recent examples of MOF work in the literature have shown that by using short DNA molecules to physically block the pores of the MOF, external triggers such as the binding of molecular analytes[32,33] or the use of restriction enzymes for degrading DNA[34] could be used to release drug molecules from within the MOFs core.

Inspired by these approaches, we hypothesized that a MOF–NAN, made by combining the highly specific protease-controlled breakdown of an outer NAN layer[10] and the pH-responsive trigger of the inner MOF, could achieve a double gated control over cargo release while simultaneously expanding the chemical nature of the cargo that the NAN could accommodate. Through the studies presented here, we show that the hybrid MOF–NAN system can indeed incorporate a greater variety of molecular cargo into its core, including small molecules, enzymes, and even plasmids while exhibiting selective control over the release conditions of the cargo. We demonstrate the extent of added control over cargo release achieved by this hybrid system using a variety of spectrometric assays and *in vitro* cell culture experiments. The MOF–NANs are shown to be non-toxic at micromolar concentrations, making them viable as cellular delivery vehicles while their outer enzyme-responsive shell enables selective release of their cargo by esterases and proteases, improving targeting of the underlying MOF structure and enabling more sensitive detection of its environment compared to single-stimuli responsive materials.

2. Experimental section

2.1 Materials

Zinc nitrate hexahydrate ($Zn(NO_3)_2{\cdot}6H_2O$, $\geq$99%), 2-methylimidazole (99%), Esterase (porcine liver esterase), Alkaline phosphatase (AP) (bovine Liver), Fluorescein (Fl) sodium salt

and methanol (HPLC grade) were purchased from Sigma-Aldrich and used as received. 5-Carboxytetramethylrhodamine (TAMRA) was obtained from Invitrogen. Camptothecin (CPT) was obtained Alfa Aesar. Azide-PEG_3-Azide crosslinker was obtained from Lumiprobe. *p*-Nitrophenolphosphate (PNPP) was purchased from EMD Millipore. Polythymidine (T20)© was purchased from Integrated© Technologies. EGFP Plasmid was obtained from OZ Biosciences. Peptide crosslinker was purchased from Genscript. The surfactant and ester crosslinker were synthesized as reported previously.[7]

2.2 Synthesis of ZIF-8 Fl, ZIF-8 TAMRA, ZIF-8 AP and ZIF-8 CPT MOFs

MOF synthesis was adapted from a previous work[12] with modifications. In a typical synthesis, zinc nitrate hexahydrate (150 mg, 0.537 mmol, 1 equiv.) and 2-methylimidazole (330 mg, 4.02 mmol, 8 equiv.) were weighed and transferred to a clean scintillation vial. Both ZIF-8 precursors are dissolved in HPLC grade methanol (7 mL). To the zinc solution, 70.8 μL of 5.5 mg mL^{-1} 5-carboxytetramethylrhodamine (5-TAMRA) stock solution in methanol was added and the resulting solution stirred for five minutes followed by dropwise incorporation of 2-methylimidazole. The reaction solution was stirred for another five minutes at room temperature or until turbidity was observed indicating the formation of ZIF-8 nanoparticles. The solution was centrifuged at 7500 rpm for 10 minutes, and the generated nanoparticles were washed three times with methanol. Loaded ZIF-8 nanoparticles were dried using vacuum centrifugation for three hours. For the synthesis of CPT-loaded and fluorescein-loaded ZIF-8, similar procedure described above was followed. The only difference was the initial combination of 2 mg of camptothecin (CPT) and 2 mg of fluorescein sodium salt with the zinc solution instead of TAMRA. For the synthesis of AP-loaded ZIF-8, 2.5 mg of Alkaline phosphatase (AP) was dissolved in deionized water.

2.3 Synthesis of ZIF-8 eGFP plasmid MOFs

Synthesis procedure was adapted from a previous work by Li and co-workers.[38] For a standard synthesis, 2-methylimidazole (23.75 mg, 0.289 mmol, 22 equiv.) was dissolved in distilled and deionized water (125 μL) was added to 25 μg of eGFP plasmid. The resulting solution was thoroughly mixed for 5 minutes at room temperature before adding 125 μL aqueous solution of zinc nitrate hexahydrate (2.4 mg, 0.0127 mmol, 1 equiv.). After 15 minutes of slow mixing, the nanoparticles were purified by centrifugation at 8000 rpm for 10 minutes and washing twice with deionized water.

2.4 Synthesis of ZIF-8 peptide surface-crosslinked micelle (SCM), MOF–SCM

Loaded ZIF-8 (0.5–1.0 mg) was weighed and dispersed in distilled and deionized water (224 μL). The ZIF-8 solution was then added to surfactant (0.8 mg, 2.11 mmol). The solution was stirred for 30 minutes at room temperature. Afterwards, CGFLGC (cathepsin B enzyme substrate) (1.25 μmol) and 2-hydroxy-4-(2-hydroxyethoxy)-2-methylpropiophenone (DHEMPP) (0.02 μmol) were included following a similar procedure to previously published methods.[10] The final solution was placed in a Rhyonet reactor for 30 minutes under constant stirring. The ZIF-8 SCMs were centrifuged at 7500 rpm for 10 minutes and washed twice with water, before re-suspending in water (250 μL).

2.5 Synthesis of ZIF-8 ester and non-ester surface-crosslinked micelle (SCM), MOF–SCM

Loaded ZIF-8 (0.5–1.0 mg) was weighed and dispersed in distilled and deionized water (224 μL). The ZIF-8 solution was then added to surfactant (0.8 mg, 2.11 mmol). The solution was stirred for 30 minutes at room temperature. Then, either ester or PEG crosslinker (0.4 μL) was added to the solution to obtain ~12 mM final concentration. Finally, Cu-THPTA (0.125 μmol) and sodium ascorbate (0.625 μmol) were introduced to the solution and stirred for 4.5 h at room temperature. The ZIF-8 SCMs were collected by centrifuging at 7500 rpm for 10 minutes, washing twice with water and re-suspending in water (250 μL).

2.6 Synthesis of ZIF-8 nucleic acid nanocapsule (NAN), MOF–NAN

Dispersed ZIF-8 SCM (5 μL), SH-polyT_{20} DNA (0.025 μmol), DHEMPP (0.02 μmol) and water (243.4 μL) were combined to obtain a final concentration of 100 μM for both surfactant and DNA. The resulting solution was placed in a Rhyonet reactor for 30 minutes. The produced nanoparticles were purified using Sephadex G-25 NAP-10 column (GE Healthcare).

2.7 Characterization of nanoparticles

For all synthesized nanomaterials, dynamic light scattering (DLS) and zeta potential measurements were performed on a Malvern Zetasizer Nano ZS System. Unstained samples for Transmission Electron Microscopy (TEM) were prepared by placing 3.0 μL of stock solution of nanoparticles onto a plasma-cleaned and carbon-coated copper grids and drying overnight. For stained samples, 80 μL of 0.5% uranyl acetate (UA) was added twice onto the copper grid prior to overnight drying. TEM imaging was conducted on a ThermoFisher Tecnai G2 Spirit BioTWIN operated at 80 keV. TEM-Energy Dispersive Spectroscopy (EDS) with ThermoFisher Talos F200X operated at 200 keV, was also used for unstained ZIF-8 SCMs. SEM images were taken using a ThermoFisher Nova NanoSEM 450 operated at 2 keV while EDS was performed at 15 keV. To generate powder XRD patterns, dried samples of loaded ZIF-8 nanoparticles were prepared by scraping the sample powder onto a sample holder and analyzed using a Rigaku Ultima IV X-ray diffractometer (Cu Kα, λ = 1.5406 Å), with a working voltage of 40 keV, a current of 44 mA and a scan speed of 2° min^{-1}.

2.8 Quantification of cargo loading

The quantification procedure was adapted from a previous work by Chen and co-workers.[27] First, 0.5–1.0 mg of dried and loaded ZIF-8 was first dispersed in 500 μL pH 5.2 sodium acetate buffer and incubated for 6 hours. The alkaline phosphatase (AP)

enzyme was isolated within the MOFs by using ultrafiltration device (Millipore, 30 K) at 14 500 rpm centrifugation for 10 minutes. The product was washed twice post synthesis with deionized water to remove remaining free 2-methylimidazole. To quantify protein loading, a Bicinchoninic Acid (BCA) assay was performed according to the protocol provided by the manufacturer. For 5-TAMRA and Camptothecin loading, different standards were prepared to generate a calibration curve. The fluorescence of 5-TAMRA (excitation: 557 nm, emission: 583 nm) and Camptothecin (excitation: 370 nm, emission: 440 nm) were measured using a BioTek Cytation 5 microplate reader. To determine the amount of the encapsulated plasmid, the free plasmid was isolated from the supernatant by ultrafiltration device (Millipore, 30 k) at 14 500 rpm centrifugation for 10 minutes. After washing twice with deionized water, the free plasmid was collected and the absorbance was read at 260 nm using a Thermo Scientific Nanodrop.

2.9 5-TAMRA release assay

The ZIF-8 TAMRA ester- or PEG-crosslinked SCM nanoparticles were incubated in three conditions: pH 5.2 + esterase, pH 7.5 + esterase, pH 5.2 + no esterase. 10 μL of 1.0 mg mL^{-1} of the stock was dispersed in either pH 5.2 sodium acetate buffer or pH 7.5 phosphate buffer saline (PBS), before adding 4 units of esterase to the first two conditions. The release of 5-TAMRA was monitored by measuring the fluorescence emission at 583 nm (excitation at 557 nm) using Biotek Cytation Imaging Reader.

2.10 Enzyme kinetics assay

Alkaline phosphatase (AP) was released from the ZIF-8 SCM construct by breaking down the ester crosslinker and incubating the nanoparticles in acidic pH. Specifically, 1.0 mg of ZIF-8 AP ester-crosslinked SCM was first dispersed in 300 μL of pH 5.2 sodium acetate buffer and followed by addition of 4 units of esterase. The solution was then incubated at 37 °C for one hour. 7.5 μL of this solution was taken and appropriate volumes of AP substrate, PNPP, (final concentrations: 100 μM, 250 μM, 500 μM, 750 μM, 1 mM) and 40 mM pH 8.0 Tris–HCl buffer with 1 mM $MgCl_2$, were added to the solution. The absorbance was read at 405 nm using a BioTek Cytation 5 microplate reader. Control experiments – esterase only and pH 5.2 only – were carried out using similar procedures.

2.11 Cell viability assay

HeLa cells were grown in DMEM supplemented with 10% FBS and 1% Penicillin/Streptomycin at 37 °C and 5% CO_2. Confluent cells were plated in a 96-well plate at 15 000 cells mL^{-1} and allowed to incubate overnight. For chloroquine treatment, cells were incubated with 25 μM chloroquine in OptiMEM for 5 hours. Cells were washed with 1× PBS. Appropriate concentrations of ZIF-8 CPT or ZIF-8 CPT NAN in OptiMEM were added, and incubated for 22 hours. 20 μL of CellTiter 96 Aqueous One Solution (Promega) was added to each well, and incubated for an additional 2 hours. Absorbance at 490 nm was measured with a BioTek Cytation 5 microplate reader.

2.12 Confocal microscopy of ZIF-8 TAMRA and ZIF-8 TAMRA NANs

HeLa cells were grown in DMEM supplemented with 10% FBS and 1% Penicillin/Streptomycin at 37 °C and 5% CO_2. Confluent cells were treated with 1 μM ZIF-8 TAMRA or ZIF-8 TAMRA NAN in OptiMEM (ThermoFisher Scientific) for 4 hours at 37 °C and 5% CO_2. Cells were then washed with 1× PBS and imaged in OptiMEM using a Leica SP8 confocal microscope. Cells were stained with Hoechst 33342 (ThermoFisher Scientific) and Lysotracker Deep Red (ThermoFisher Scientific) prior to imaging, following the protocol provided by the manufacturer.

2.13 Confocal microscopy of ZIF-8 EGFP Plasmid NANs

HeLa cells were grown in DMEM supplemented with 10% FBS and 1% Penicillin/Streptomycin at 37 °C and 5% CO_2. Confluent cells were treated with either 10.25 μM peptide-crosslinked NANs containing ~35 μg mL^{-1} plasmid MOFs, 10.00 μM ester-crosslinked NANs containing ~34 μg mL^{-1} plasmid MOFs, or 10 μM non-ester-crosslinked NANs containing ~34 μg mL^{-1} plasmid MOFs in OptiMEM for 4 hours 37 °C and 5% CO_2. Cells were washed with 1× PBS and incubated an additional 20 hours in DMEM supplemented with 10% FBS. Cells were washed with 1× PBS and imaged in OptiMEM. Cells were stained with Lysotracker Deep Red and Hoechst 33342 prior to imaging. Images were using a Leica SP8 confocal microscope.

3. Results and discussion

3.1 Synthesis of MOF–NAN nanoparticles

To assemble the MOF–NAN particles, ZIF-8 MOFs are synthesized from 2-methyl imidazole and $Zn(NO_3)_2$ according to established literature protocols.[17] A multi-alkyne presenting surfactant (1)[7] is added in excess of the ZIF-8 MOFs, resuspended in water. The self-assembly of the surfactant around the MOF is anticipated to be driven by the hydrophobic nature of the 2-methyl imidazole ligands that comprise the ZIF-8's surface. The resulting structure, once given sufficient time to assemble, is added to a solution of crosslinker composed of either an azide-modified ester crosslinker or a thiolated peptide, and reacted at the micelle surface either using a Cu-catalyzed azide–alkyne cycloaddition reaction or by stepwise thiol–yne reactions to generate surface crosslinked micelles (SCM) around the ZIF-8 MOFs, respectively (Fig. 1).

The ester crosslinker (2) is used as a target for esterase enzymes[7] and the peptide crosslinkers are used for selective protease triggered degradation.[10] For the peptide-crosslinked NAN studies described here, we designed the peptide crosslinker with the embedded amino acid motif GFLG, as it is the substrate of the endosomal enzyme Cathepsin B (CathB). A full list of the crosslinkers used in this study can be found in Fig. S1, ESI.†

3.2 Characterization of MOF–NAN nanoparticles

Characterization of the resulting ZIF-8 MOF–NANs was achieved using a variety of nanocharacterization techniques, including, transmission electron microscopy (TEM), scanning

electron microscopy (SEM), dynamic light scattering (DLS), X-ray powder diffraction (XRD) and energy dispersive X-ray spectroscopy (EDS) analysis (Fig. 2).

XRD confirmed that the lattice structure of the ZIF-8 MOF was maintained during the encapsulation within the NAN. Once encapsulated, it was of particular interest to monitor the stability of the MOFs structure post treatment with stabilizing surfactants and the subsequent chemical crosslinking of the surfactants (Fig. 2C and Fig. S2–S4A, ESI†). EDS confirmed the presence of zinc and nitrogen from the metal ions and carbon was present from the organic ligands and surfactants of the MOF within the surface crosslinked micelle (MOF–SCM) (Fig. 2B). The average size of the ester-crosslinked MOF–SCMs in solution was determined to be roughly 10 nm using DLS (Fig. 2A) and samples observed by SEM indicated a range of diameters from 20–50 nm when dried (Fig. 2D and Fig. S3C, ESI†). Full DLS and zeta potential measurements for all particles can be found in Table S1, ESI.† The size of a MOF–SCM construct was shown to vary slightly depending upon the extent and type of cargo loaded and the crosslinker used in the SCM shell.

To determine the extent of added chemical stability that the surfactant micelle layer provided to the ZIF-8 MOFs, the particles were synthesized with carboxy-fluorescein dye encapsulated within the MOFs core. Carboxy-fluorescein dye was selected for use in the gel mobility shift assay due to its mobility under an electric field due to its negative charge.

Fluorescein-MOFs (Fl-MOFs) were further encapsulated in an ester-crosslinked SCM, and then functionalized with DNA to generate the complete MOF–nucleic acid nanocapsule (MOF–NAN) system (Fig. 3A). Post addition of DNA to the MOF–SCM surface the particles increased in size and had a zeta potential of −30 mV, indicative of DNA functionalization at the surface (Fig. 3B).[7] Using the gel mobility shift assay in an agarose gel, it was shown that the fluorescein dye within the ZIF-8 MOFs was readily released into solution when placed in the gel buffer containing the metal chelator EDTA, whereas the fluorescein dye-loaded ZIF-8 MOFs encapsulated within the NANs did not show any release of the dye (Fig. 3A). This indicated that the EDTA could not access the Zn^{2+} ions within the MOF due to successful encapsulation within the NAN's micelle core. To investigate the uptake of the particles into cells, HeLa cells were incubated with TAMRA loaded MOF NANs (Fig. 3C). Using lysotracker red to highlight the presence of the cells

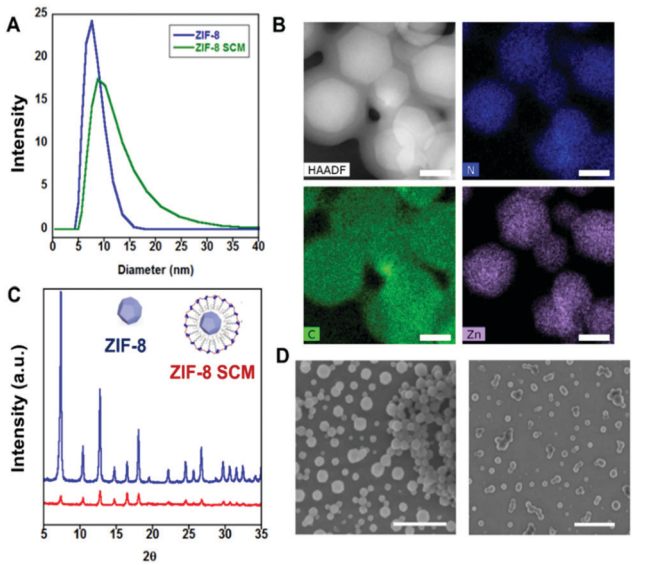

Fig. 2 Nanoscale characterization of ZIF-8 MOF encased in surface crosslinked micelles (SCMs). (A) DLS pre- and post encapsulation of a ZIF-8 MOF in a crosslinked surfactant shell. (B) Compositional analysis of MOF–SCMs by EDS showing the presence of zinc and nitrogen from a ZIF-8 lattice and carbon from the SCM shell, all scale bars 50 nm. (C) XRD analysis indicating the retention of ZIF-8 crystallinity after encapsulation in the SCM. (D) Scanning electron microscopy of ZIF-8 MOFs pre (left) and post (right) encapsulation in a SCM. Scale bars are 400 nm (left) and 1 μm (right), respectively.

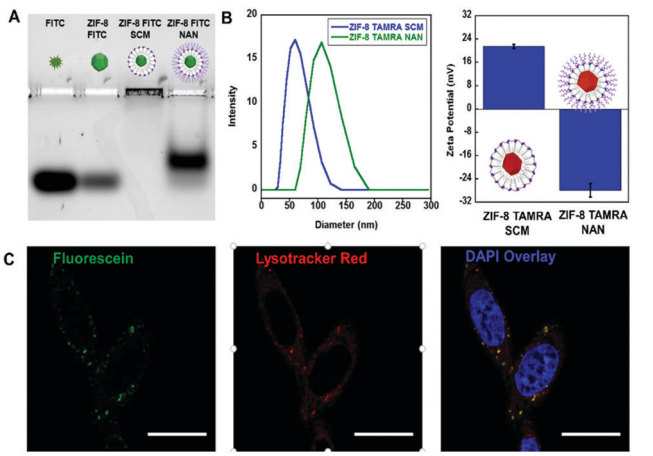

Fig. 3 Assembly of dye loaded ZIF-8 MOFs encapsulated in NANs built from crosslinked DNA-surfactants. (A) Gel electrophoresis (0.5% agarose) showing the stability of fluorescein-loaded ZIF-8 MOFs post encapsulation in an SCM or NAN compared to unencapsulated fluorescein-loaded ZIF-8 MOFs. First lane is free carboxy-fluorescein dye as a reference which is repelled by the negative electrode (located at top of gel). Second lane shows that loading of the dye into a ZIF-8 MOF does not affect the dyes mobility as the MOF degrades and releases the dye in the gels loading buffer as it contains the metal chelator EDTA. The third lane shows that encapsulation in a positively charged MOF–SCM prevents the dyes mobility into the gel, and that the MOF can no longer degrade because of the micelle outer layer. Note: We have observed that SCMs with heavier cargo such as MOFs tend to aggregate in high ionic strength solutions such as gel loading buffer and PBS. In lane four, further functionalization of the fluorescein-loaded ZIF-8 MOF SCMs with poly T20 DNA ligands to generate a ZIF-8 MOF NAN enables mobility of the entire structure through the 0.50% agarose gel as the DNA ligands help with solubility in the gel's loading buffer. The DNA also provides a negatively charged surface that repels the structure from the negative electrode. The mobility is in the same direction as the free dye, but the added mass of the ZIF-8 MOF–NAN structure limits its total electrophoretic mobility. (B) Increase in particle size as seen by DLS (left) and negative shift in zeta potential (right) indicates successful covalent attachment of DNA ligands on to a TAMRA-loaded SCM surface *via* thio–lyne photo crosslinking step (see Experimental section for details) The surface change to −30 mV is indicative of full coverage of the surface of the NAN layer with DNA. (C) Confocal microscopy of HeLa cells incubated with 1 μM ZIF-8 TAMRA NANs, scale bars 20 μm. Fluorescein channel highlights presence of TAMRA dye in MOF–NAN interior (left image), lysotracker red highlights endosomal compartments (middle image) and the DAPI channel highlights the cell's nucleus stained with Hoechst stain (right image).

endosomes it was shown that the MOF–NANs colocalized within endosomes. In addition, TAMRA MOF NANs were compared to unencapsulated TAMRA MOFs (Fig. S4B, ESI†). This study showed that although the MOFs entered cells effectively, there was a significant amount of debris that was observed in the cell culture dish that is attributed to the instability of the MOFs in serum, whereas the MOF–NANs under similar conditions did not present any debris. This was attributed to the added stability provided by the surface crosslinked NAN shell encapsulating the MOFs.

3.3 Dual gated release study

Next, in order to test degradation of the individual layers of the MOF–SCMs, a second dye, TAMRA, was encapsulated within the MOF and this dye-loaded MOF further encapsulated within an ester-crosslinked SCM (Fig. 4). Different stimuli were then introduced to the dye-loaded MOF–SCMs to determine the level of control each layer (MOF, SCM) contributed to the overall stability of the hybrid structure. As shown in Fig. 4B, the ester-crosslinked TAMRA-loaded MOF SCMs only release the TAMRA dye from its interior when both triggers are present (low pH and esterase). These two triggers were designed into the system as they are both consistent with cellular endosomal environments (acidification of endosomes as they mature, and the presence of endosomal esterases). As can be seen in Fig. 4C, TEM indicates that compared to MOF–SCMs synthesized with the biodegradable ester crosslinker, those synthesized with a non-degradable short polyethylene glycol (PEG) crosslinker remain intact post treatment with esterase enzymes and acid treatment.

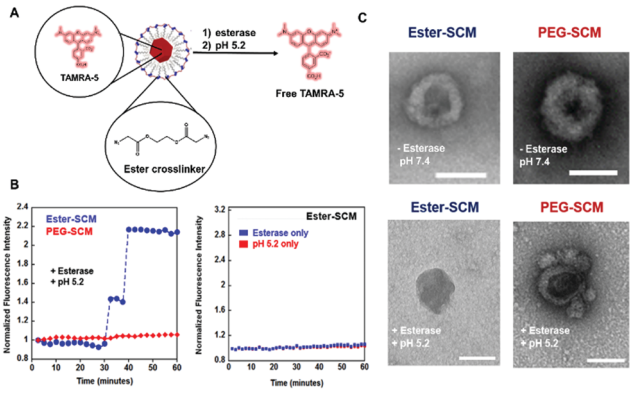

Fig. 4 Double gated release of dye molecules from ZIF-8 MOF–SCMs. (A) The release of TAMRA dye is achieved by treating the ZIF-8 MOF SCMs with esterase to cleave the crosslinker followed by pH 5.2 to disintegrate the ZIF-8 MOF. (B) TAMRA release is only observed for ester-crosslinked TAMRA ZIF-8 MOF SCMs, (0.167 mg ZIF-8 TAMRA mL^{-1}) after one hour incubation in 4 units of esterase and pH 5.2, no dye release observed from PEG-crosslinked TAMRA MOF SCMs. (C) Left panel: TEM image of ester crosslinked SCMs pre (top) and post (bottom) degradation of ester-crosslinked TAMRA ZIF-8 MOF SCM after one hour treatment with esterase and pH 5.2. Right panel: TEM images of intact PEG-crosslinked TAMRA ZIF-8 MOF SCMs both before (top) and after (bottom) one hour treatment with esterase and pH 5.2. All scale bars are 100 nm and all samples stained with uranyl acetate for contrast. In both (C) (top images), and Fig. 1D, the initial coverage of soft material encasing the ZIF-8 MOF (as highlighted by the uranyl acetate staining) is removed by treatment with acid and enzyme. The underlying ZIF-8 can be observed in stable condition post removal of the surfactant and nucleic acid ligands as seen in (C) (bottom images).

3.4 Protein encapsulation and release study

In order to test the capacity of the NAN to accommodate larger hydrophilic cargo *via* introduction of a MOF core, a ZIF-8 MOF was loaded with protein cargo and further encapsulated into the NAN's interior. To investigate its degradation properties the enzyme alkaline phosphatase (AP) was incorporated. AP is an enzyme that can readily and rapidly dephosphorylate various substrates. For our assay, we specifically chose a substrate commonly used in a coulometric test of phosphatase enzymatic activity. First the successful encapsulation of AP enzyme within the MOF was confirmed using Coomassie blue stain in 7.5% SDS-PAGE gel (Fig. S5, ESI†) and the structure of the MOF analyzed using XRD (Fig. S2B and S3, ESI†). It was found by XRD that there are some changes in the crystallinity pattern when AP is incorporated. Therefore, it was next tested whether the enzymes activity remained intact post encapsulation and whether its activity can be regulated by further encapsulation within the NAN outer shell, using the initially colorless substrate *para*-nitrophenol phosphate (PNPP), a substrate which is rapidly hydrolyzed by AP to a bright yellow *para*-nitrophenol (PNP) product (Fig. 5B), we evaluated the ability of the enzyme to access the PNPP substrate while embedded within the MOF–SCM. By doing so we sought to determine the effects of encapsulation on the enzymes turn over kinetics and correlate rate effects as an indirect read out of the stability of each layer of the MOF–SCM. Using this assay, we observed that the AP enzyme within the MOF–SCM had no activity when treated with PNPP compared to AP enzyme encased in the ZIF-8 MOF, which maintained its ability to convert PNP to PN (Fig. S9, ESI†) attributed to diffusion of PNPP into the MOF pores. In addition, we found that post treatment with acid, the AP–MOF could recover its activity completely. However, the AP–MOF–SCMs treated with acid did not regain activity, suggesting that the outer crosslinked micelle prevented activity of the enzyme (Fig. 5C).

Next the AP–MOF–SCMs were treated with esterase, which can break the crosslinkages of the SCMs outer surface linkages. Despite addition of esterase at pH 7, the production of the PN product remained limited. However, after dropping the pH to 5.2 to release the AP, we found that the rate of product formation rapidly increased, indicating the loss of the MOF cage around the enzyme, a result which correlated well with what was observed by gel electrophoresis using the fluorescein-loaded MOF–NANs. Importantly, the enzyme post release from the MOF–SCM system converted PNPP to PNP with kinetic parameters (Table S3, ESI†) comparable to the reported values in literature,[35] despite the presence of esterase and subjecting the sample to acidic conditions. As esterase operates most effectively under acidic pH and could also potentially hydrolyze the PNP substrate (albeit at a slower rate than the AP enzyme), we background subtracted any cleavage observed in the esterase-only case. The activity of the substrate in the presence of just the esterase enzyme at pH 5.2 can be seen in Fig. 5C. The normalized rates of PNPP hydrolysis and the saturation of the enzymes activity at high concentrations of substrate are shown

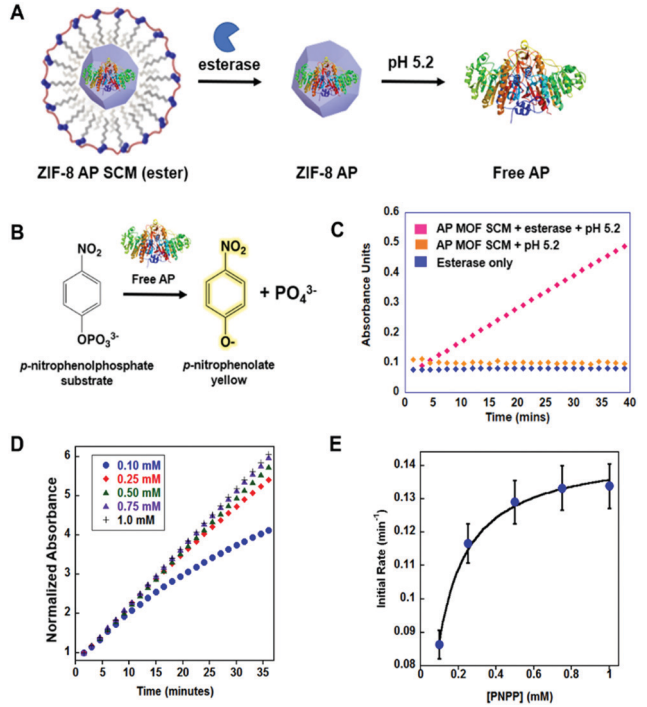

Fig. 5 Kinetics of alkaline phosphatase (AP) liberated from ZIF-8 SCMs. (A) Release of AP from ZIF-8 SCM construct *via* treatment with esterase and pH 5.2. (B) Standard PNPP hydrolysis assay using AP. (C) PNPP hydrolysis assay in the presence of AP MOF–SCMs where [PNPP] = 0.75 mM, showing that only in the presence of esterase and pH 5.2 that AP within the MOF–SCMs can be released and catalyze the PNPP hydrolysis. Esterase and PNPP only shown in blue as a control for background hydrolysis. (D) Representative data for PNPP hydrolysis assay by AP enzyme post release from a ZIF-8 SCM, see Fig. S8, ESI† for two additional trials. (E) Rate analysis of PNPP hydrolysis at a fixed concentration of enzyme [0.150 mM AP] (0.10 mg mL^{-1} ZIF-8 AP SCM). Error bars are generated from the three trials.

in Fig. 5D and E, respectively. These results indicated yet again that the individual stimuli-responsive cues for each material layer were intact and could be individually triggered, helping to regulate access of the core contents of the MOF–NANs to the surrounding solution, including large biomacromolecules such as proteins.

3.5 *In vitro* activity of MOF–NANs

After establishing that the MOF–SCMs required sequential acidic and enzymatic triggers to be present in order to fully degrade the MOF core and release its contents, MOF–NANs were evaluated for their toxicity in cells to determine if the hybrid multilayered nanomaterial could serve as a highly controlled cargo delivery system for live cells. Toxicity was quantitatively evaluated using a standard MTS assay (Promega). The results showed that treatment with MOF–NANs is non-toxic up to 20 μM in HeLa cells (Fig. 6A), indicating their potential for cellular applications. To analyze the double-gated control over cellular delivery of a small molecule cargo, the cytotoxic drug camptothecin (CPT) was incorporated into the MOFs and further encapsulated by a NAN.

Results of these experiments and their characterization by TEM, SEM and confocal microscopy can be seen in Fig. 6. CPT–MOF–NANs were incubated with HeLa cells and shown to have a dose-dependent toxicity (Fig. 6A). The CPT–MOF–NANs were then evaluated using various crosslinkers to determine the ability of the hybrid MOF–NAN to release their cargo depending on the chemical make-up of each layer of the construct and which stimuli were present, assessed through a standard MTS assay.

The results showed that 20 μM MOF–NANs (with an effective CPT concentration of 80 nM) successfully reduced cell viability by roughly 40% compared to that of untreated cells (Fig. 6A). These results indicate that the MOF–NANs could successfully deliver small hydrophobic molecules into cells *via* the sequential degradation of the NAN and the MOF layers. However, the question remained whether or not the outer layer of the NAN was providing additional chemical stability for the ZIF-8 framework in the interior of cells and thus a potentially safer route of drug administration as compared to that of the bare ZIF-8 MOF. To test this concept, CPT-loaded MOF–NANs were synthesized with a biodegradable (peptide crosslinked) SCM shell, then incubated with HeLa cells. Their toxicity was then compared to that of PEG-crosslinked (non-degradable) MOF NANs. As seen in Fig. 6B, the PEG crosslinked MOF NANs exhibited negligible toxicity in cells despite loading them with CPT. To further investigate the role of pH in CPT's release, we co-incubated MOF–NANs and HeLa cells with chloroquine, a chemical known to halt the acidification of the endosome.[36] As shown in Fig. 6B, upon the addition of chloroquine both the bare CPT–MOFs and CPT–MOF–NANs exhibited little or no cytotoxicity, highlighting that the additional acid catalyzed degradation of the MOF within the NAN is necessary intracellularly in addition to esterase mediated degradation of the NAN's outer shell to achieve more complete release of the internalized cargo. This result indicates an additional level of stability of the ZIF-8 MOFs made possible by the MOF's outer NAN layer. These results have important implications for successfully delivering cytotoxic drugs, and may help to addresses the outstanding issues surrounding premature leakage of cargo from MOFs in cellular systems.

3.6 Plasmid delivery using MOF–NAN

Lastly, after observing the additional stability that the MOF–SCM and MOF–NANs maintained both *in vitro* and in cell culture for delivering small molecular cargo, we investigated the ability of the MOF–NAN system to deliver a large hydrophilic cargo in a controlled fashion. To test this, we paired the composition of the NANs outer shell and the interior MOF-character for enzyme-triggered release and plasmid encapsulation, respectively. For this assay, we incorporated a DNA plasmid that encodes enhanced green fluorescent protein (eGFP), which if successfully delivered into cells would translate and express the bright fluorescent protein eGFP, a protein commonly used for biological tracking and labeling experiments.[37] eGFP has a bright emission band at 520 nm. Encapsulation of the eGFP plasmid in the ZIF-8 MOF was prepared using a previously published method for encapsulation of plasmids in MOFs.[38]

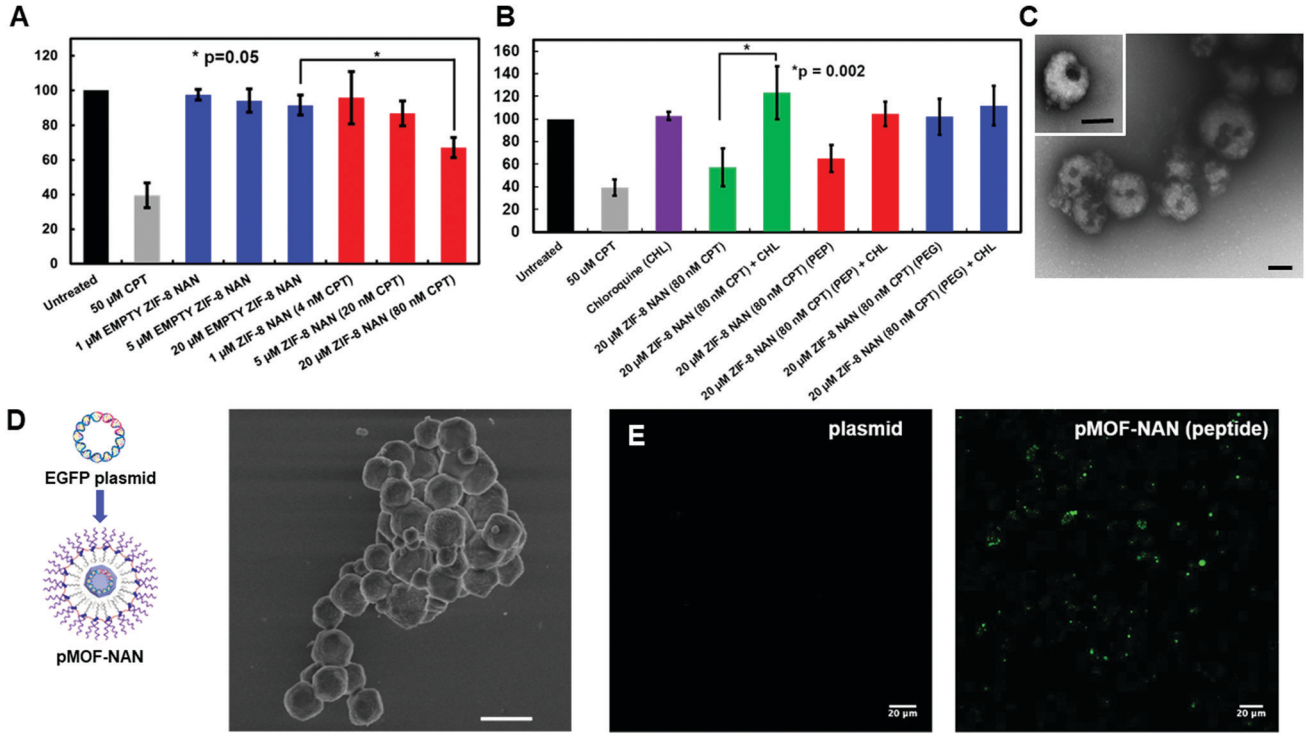

Fig. 6 Cellular activity of MOF–NANs containing camptothecin (CPT). (A) Cellular toxicity of empty MOF–NANs *vs.* MOF–NANs with increasing concentration of CPT encapsulated. Error bars are generated from three trials. (B) The effects of chloroquine on toxicity of CPT-loaded MOF NANs and MOFs along with the toxicity of CPT loaded MOF NANs tethered with a peptide (GFLG) *vs.* PEG SCM crosslinkers. Error bars are generated from three trials. (C) TEM image of MOF SCMs crosslinked with GFLG peptide motif, scale bars 100 nm. (D) Plasmid loaded NANs, pMOF–NAN assembly (left), SEM image of pMOFs (right), scale bar 1 μm. (E) Confocal microscopy of plasmid uptake and expression in HeLa cells for just the plasmid alone (left) and plasmid delivered *via* MOF–NANs crosslinked with GFLG peptides (~0.77 μg plasmid).

The resulting plasmid MOFs (pMOFs) were characterized by TEM and XRD and shown to maintain a similar crystallinity to that of the parent ZIF-8 MOF (Fig. 6D and Fig. S2A, ESI†). We then treated HeLa cells with eGFP plasmid MOF–NANs (pMOF–NAN). Post cell incubation of the pMOF–NANs for 4 hours, the cells were washed of excess particles and analyzed by confocal microscopy for evidence of eGFP expression (Fig. 6E). Peptide-crosslinked NANs showed expression of the eGFP protein after enough time was allotted for proteins to be translated (20 h) in contrast to bare plasmid delivery. As a negative control for the enzyme responsive nature of the pMOF–NAN degradation, PEG-crosslinked pMOF NANs were synthesized and assessed in HeLa cells. No green fluorescence was observed (Fig. S10, ESI†). These results show that the ability to not only stabilize the plasmid for cellular uptake and delivery but to incorporate a large anionic oligonucleotide into the MOF–NAN structure, can enable a highly controllable delivery platform for introducing plasmids into cells in an enzyme-responsive and highly programmable fashion.

4. Conclusions

In summary, we have shown that incorporation of a MOF into the core of a DNA-surfactant assembled micelle resulted in a greater breath of molecular cargo that can be accommodated into the nucleic acid nanocapsule formulation while simultaneously imparting improved chemical stability to a MOF under biological conditions. Additionally, it was shown that the NAN's outer shell enables a greater degree of control over the accessibility of the MOFs interior to its environment, requiring specific enzymes to be present alongside acidic conditions in order to release encapsulated cargo. This double gated release mechanism results in a greater degree of control with regards to both enzyme activity and cellular delivery assays involving MOFs, indicating a broad range of potential applications for this unique hybrid nanostructure.

Conflicts of interest

The authors declare no conflict of interest.

Acknowledgements

The authors would like to gratefully acknowledge funding from NSF grant 1847869 for supporting this work, and Jared Fee and Dr Steven Suib at the University of Connecticut for assistance with the XRD analysis of the MOF structures in this work. We would also like to acknowledge the Biosciences Electron Microscopy Laboratory (BEML) which provided the Leica SP8

(acquired under NIH grant S10OD016435) for confocal imaging carried out in this work.

References

1 S. Kalepu and V. Nekkanti, *Acta Pharm. Sin. B*, 2015, **5**, 442.
2 W. G. Pitt and G. Husseini, *Adv. Drug Delivery Rev.*, 2008, **60**, 1137.
3 T. Wei, J. Liu, H. Ma, Q. Cheng, Y. Huang, J. Zhao, S. Huo, X. Xue, Z. Liang and X. Liang, *Nano Lett.*, 2013, **13**, 2528.
4 O. L. Ramos, R. N. Periera, L. S. Simoes, D. A. Madalena, R. M. Rodrigues, J. A. Teixeira and A. A. Vincente, in *Biopolymer Nanostructures for Food Encapsulation Purposes: Nanoencapsulation in Food Industry*, ed. S. M. Jafari, Elsevier, Amsterdam, 1st edn, 2019, ch. 3, vol. 1, pp. 69–100.
5 B. J. Bruno, G. D. Miller and C. S. Lim, *Ther. Delivery*, 2013, **4**, 1443.
6 H. Song, M. Yu, Y. Lu, Z. Gu, Y. Yang, M. Zhang, J. Fu and C. Yu, *J. Am. Chem. Soc.*, 2017, **139**(50), 18247.
7 J. K. Awino, S. Gudipati, A. K. Hartmann, J. J. Santiana, D. F. Cairns-Gibson, N. Gomez and J. L. Rouge, *J. Am. Chem. Soc.*, 2017, **139**, 6278.
8 A. K. Hartmann, D. F. Cairns-Gibson, J. J. Santiana, M. Tolentino, H. M. Barber and J. L. Rouge, *ChemBioChem*, 2018, **19**, 1734.
9 J. I. Cutler, E. Auyeung and C. A. Mirkin Rouge, *J. Am. Chem. Soc.*, 2012, **134**, 1376.
10 J. J. Santiana, B. Sui, N. Gomez and J. L. Rouge, *Bioconjugate Chem.*, 2017, **28**, 2910.
11 K. Liang, R. Ricco, D. M. Doherty, M. J. Styles, S. Bell, N. Kirby, S. Mudie, D. Haylock, A. J. Hill, C. J. Doonan and P. Falcaro, *Nat. Commun.*, 2015, **6**, 7240.
12 Y. Liu, Y. Zhao and X. Chen, *Theranostics*, 2019, **9**, 3122.
13 C. Doonan, R. Ricco, K. Liang, D. Bradshaw and P. Falcaro, *Acc. Chem. Res.*, 2017, **50**, 1423.
14 J. Feng, Z. Xu, P. Dong, W. Yu, F. Liu, Q. Jiang, F. Wang and X. Liu, *J. Mater. Chem. B*, 2019, **7**, 994.
15 H. Zheng, Y. Zhang, L. Liu, W. Wan, P. Guo, A. M. Nystrom and X. Zou, *J. Am. Chem. Soc.*, 2016, **138**, 962.
16 Z. Liang, Z. Yang, H. Yuan, C. Wang, J. Qi, K. Liu, R. Cao and H. Zheng, *Dalton Trans.*, 2018, **47**, 10223.
17 S. Peng, B. Bie, Y. Sun, M. Liu, H. Cong, W. Zhou, Y. Xia, H. Tang, H. Deng and X. Zhou, *Nat. Commun.*, 2018, **9**, 1293.
18 J. Zhuang, C. H. Kuo, L. Y. Chou, L. De-Yu, E. Weerapana and C. K. Tsung, *ACS Nano*, 2014, **8**, 2812.
19 M. A. Luzuriaga, R. P. Welch, M. Dharmarwardana, C. E. Benjamin, S. Li, A. Shahrivarkevishahi, S. Popal, L. H. Tuong, C. T. Creswell and J. J. Gassensmith, *ACS Appl. Mater. Interfaces*, 2019, **11**(10), 9740.
20 S. Li, X. Zhou, Z. Chen, F. C. Herbert, R. Jayawickramage, S. D. Pangangala, M. A. Luzuriaga, S. B. Alahakoon, S. D. Diwakara, X. Meng, L. Fei, J. Ferraris, R. A. Smaldone and J. J. Gassensmith, *ACS Appl. Mater. Interfaces*, 2020, **12**(10), 11884–11889.
21 K. Liang, J. J. Richardson, C. J. Doonan, X. Mulet, Y. Ju, J. Cui, F. Caruso and P. Falcaro, *Angew. Chem., Int. Ed.*, 2017, **56**, 8510.
22 Y. Duan, X. Feng, X. Yang, W. Sun, Y. Jin, H. Liu, K. Ge, Z. Li and J. Zhang, *Biomaterials*, 2017, **122**, 23.
23 Q.-S. Pan, T.-T. Chen, C.-P. Nie, J.-T. Yi, C. Liu, Y.-L. Hu and X. Chu, *ACS Appl. Mater. Interfaces*, 2018, **10**, 33070.
24 S. K. Alsaiari, S. Patil, M. Alyami, K. O. Alamoudi, F. A. Aleisa, J. S. Merzaban, M. Li and N. M. Khashab, *J. Am. Chem. Soc.*, 2018, **140**(1), 143.
25 W. Cai, J. Wang, C. Chu, W. Chen, C. Wu and G. Liu, *Adv. Sci.*, 2019, **6**, 1801526.
26 M. A. Luzuriaga, C. E. Benjamin, M. W. Gaertner, H. Lee, F. C. Herbert, S. Mallick and J. J. Gassensmith, *Supramol. Chem.*, 2019, **31**, 485.
27 T. T. Chen, J. T. Yi, Y. Y. Zhao and X. Chu, *J. Am. Chem. Soc.*, 2018, **140**, 9912.
28 B. Illes, P. Hirschle, S. Barnert, V. Cauda, S. Wuttke and H. Engelke, *Chem. Mater.*, 2017, **29**, 8042.
29 H. Zhang, Q. Li, R. Liu, X. Zhang, Z. Li and Y. Luan, *Adv. Funct. Mater.*, 2018, **28**, 1802830.
30 D. Rosenblum, N. Joshi, W. Tao, J. M. Karp and D. Peer, *Nat. Commun.*, 2018, **9**, 1410.
31 Y. Pan, D. Heryadi, F. Zhou, L. Zhao, G. Lestari, H. Su and Z. Lai, *CrystEngComm*, 2011, **13**, 6937.
32 J. S. Kahn, L. Freage, N. Enkin, M. A. A. Garcia and I. Willner, *Adv. Mater.*, 2017, **29**, 1602782.
33 W.-H. Chen, W.-C. Liao, Y. S. Sohn, M. Fadeev, A. Cecconello, R. Nechushtai and I. Willner, *Adv. Funct. Mater.*, 2018, **28**, 1705137.
34 W. H. Chen, G.-F. Luo, Y. S. Sohn, R. Nechushtai and I. Willner, *Adv. Funct. Mater.*, 2019, **29**, 1805341.
35 R. L. Dean, *Biochem. Mol. Biol. Educ.*, 2002, **30**, 401.
36 R. E. Chapman and S. Munro, *EMBO J.*, 1994, **13**, 2305.
37 U. Schnell, F. Dijk, K. A. Sjollema and B. N. G. Giepmans, *Nat. Methods*, 2012, **9**, 152.
38 Y. Li, K. Zhang, P. Liu, M. Chen, Y. Zhong, Q. Ye, M. Q. Wei, H. Zhao and Z. Tang, *Adv. Mater.*, 2019, **31**, 1901570.